REVIEW

Phosphor-converted light-emitting diodes in the marine environment: current status and future trends

Maofeng Hua,[a] Shuifu Liu,[ab] Lei Zhou, [ID] *[a] Jean-Claude Bünzli [ID] *[cd] and Mingmei Wu [ID] *[a]

The exploitation and utilization of resources in marine environments have ignited a demand for advanced illumination and optical communication technologies. Light-emitting diodes (LEDs), heralded as "green lighting sources", offer a compelling solution to the technical challenges of marine exploration due to their inherent advantages. Among the myriad of LED technologies, phosphor-converted light-emitting diodes (pc-LEDs) have emerged as frontrunners in marine applications. At the heart of pc-LEDs lie phosphor materials, colour-converters that orchestrate the emission of light. In the marine environment, blue-green light with a wavelength of 440−570 nm exhibits the deepest penetration depth, while other wavelengths are rapidly attenuated in the shallow layer. Additionally, specific wavelengths of light are crucial for particular applications. However, the moist marine environment as well as the demand for continuous and stable lighting pose a formidable challenge to the environmental stability of the phosphors. Therefore, developing blue-green phosphors with exceptional colour purity and high thermal and moisture stability is paramount for marine applications. Herein, this review delves into the application of LED and pc-LED technology in underwater optical communication and marine fishery, exploring the development strategies of phosphors tailored for the marine environment. The insights presented serve as a valuable reference for further research on phosphors and pc-LED devices.

1 Introduction

The relentless pursuit of sustainable development has propelled coastal nations towards the rational exploitation and utilization of marine resources, fostering a vibrant marine economy. Solid-state lighting technology has emerged as a transformative force in this endeavor, offering innovative solutions for both underwater and surface marine applications, such as light communications and marine fishery.[1–4] Primary traditional marine lighting devices, relying on incandescent and metal halide (MH) lamps, are plagued by inherent drawbacks, including exorbitant energy consumption, limited lifespan and inefficient performances. More sustainable alternatives, for instance, light-emitting diodes (LEDs), especially the white light-emitting diodes (WLEDs) are now replacing obsolete light sources, establishing themselves as the

frontrunners in marine applications due to their exceptional longevity, low energy consumption, minimal heat radiation, and rapid response time.[5–8]

WLEDs can be fabricated through two primary approaches: either by combining three primary-colour (red/green/blue) LEDs or by employing phosphor-converted LEDs (pc-LEDs) to transform the blue or near-ultraviolet (n-UV) emission of a single LED chip into white light.[6,9] The latter approach offers compelling advantages over the former in terms of cost-effectiveness and manufacturing simplicity. Beyond white light, pc-LEDs fitted with adequate phosphors can also transform the short-wavelength emission from LED chips into a spectrum tailored to specific applications.[10,11] Moreover, pc-LEDs can be tailored with specific phosphors to emit wavelengths suited for various marine applications, enhancing energy efficiency beyond the capabilities of traditional white light sources. In addition, the marine environment, with its pervasive humidity and salinity, poses a formidable challenge to the stability of phosphors. To ensure the longevity and reliability of pc-LEDs in marine applications, phosphor materials must be meticulously engineered. This necessitates the development of anti-thermal-quenching and moisture-resistant phosphors that retain their luminescent properties whatever the environment they are working in.

[a]*Zhuhai Key Laboratory of Optoelectronic Functional Materials and Membrane Technology, School of Chemical Engineering and Technology, Sun Yat-sen University, Zhuhai, 519082, P. R. China. E-mail: zhoul8@mail.sysu.edu.cn; ceswmm@mail.sysu.edu.cn*

[b]*College of Materials, Xiamen University, Xiamen 361005, P. R. China*

[c]*Department of Applied Biology and Chemical Technology, The Hong Kong Polytechnic University, Kowloon, Hong Kong, 999077, P. R. China*

[d]*Institute of Chemical Sciences and Engineering, Swiss Federal Institute of Technology Lausanne (EPFL), Lausanne, Switzerland. E-mail: jean-claude.bunzli@epfl.ch*

Significant advances in pc-LED technology have been achieved recently but there is a lack of comprehensive reviews interweaving the application of LED devices with the development of phosphor materials for the marine environment. This paper aims to bridge this gap by providing an overarching perspective on the role of pc-LEDs in the marine field, delving into the specific requirements of marine applications, and reviewing the development of high-performance phosphors for pc-LEDs (Fig. 1). It also intends to serve as a valuable reference for researchers and practitioners alike, paving the way for the transformative application of pc-LEDs in the marine field.

2 Application of pc-LEDs in marine environments

2.1 Underwater wireless optical communications (UWOC)

Traditional wireless communication modes, such as acoustic communications and radio communications, are often limited in their ability to simultaneously achieve high-speed and long-distance transmission. Visible light communications (VLC) have emerged as a promising alternative for maritime applications due to their adjustable bandwidth and long transmission distance.[13,14] Additionally, the visible-light band, with a spectral range between 380 and 780 nm, is unlicensed, unlike radio frequencies, allowing for utilization without authorization, and it also ensures high privacy and safety since it is not sensitive to electromagnetic interferences.[15] Underwater wireless optical communications (UWOC) have the potential to play a significant role in a wide range of applications, including tactical surveillance, pollution monitoring, oil control and maintenance, offshore explorations, climate change monitoring, and oceanographic research.[16] A typical UWOC system can be divided into three main components: the transmitter unit, the water channel, and the receiver module. Laser diodes (LDs) or LEDs are commonly employed as receivers and transmitters in UWOC systems (Fig. 2a). Moreover, LEDs offer advantages in terms of cost, and lifetime in comparison to LDs.[17] In a LED-based UWOC system, a photoelectric conversion device is incorporated into the receiver to convert the transmitted light signal into electric signal.

Recently, pc-LED devices have gained interest in UWOC applications. However, the quantum-confined stark effect (QCSE) of the InGaN/GaN LED quantum wells and phosphor materials pose a challenge, limiting the modulation bandwidth.[18,19] To address this issue and improve data transmission rates, several solutions have been proposed, which include the
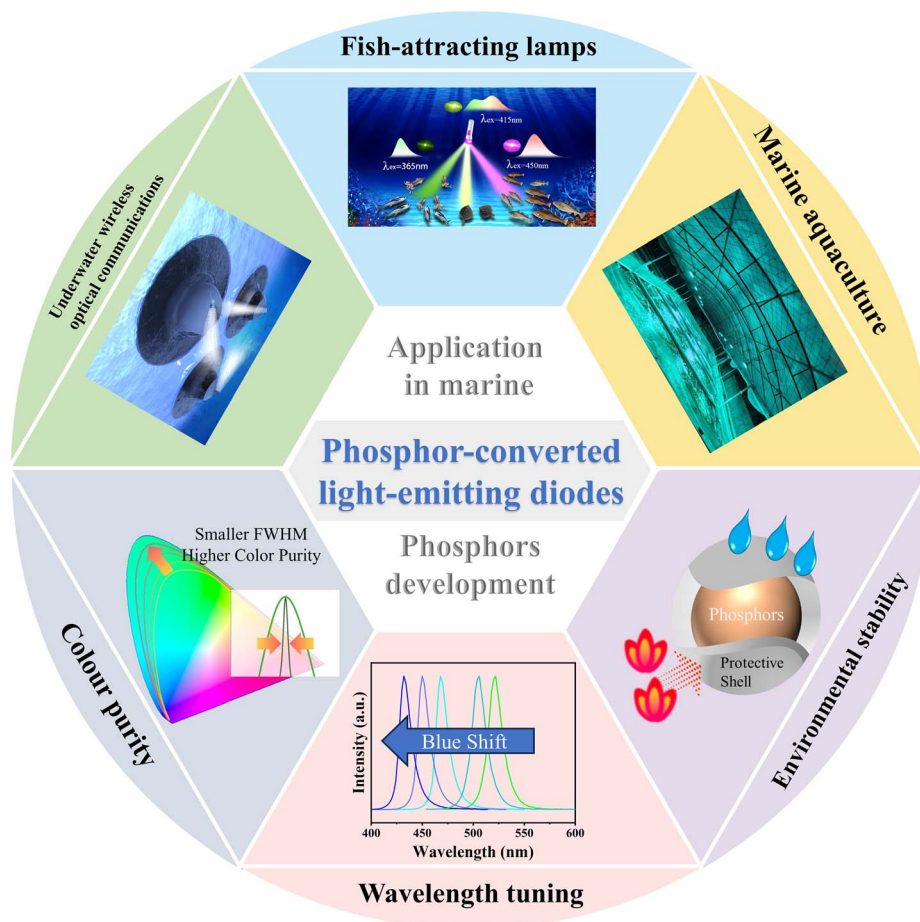

Fig. 1 Research content of this review. The figure in the section of colour purity is reprinted with permission from ref. 12. Copyright 2021, Springer Nature.
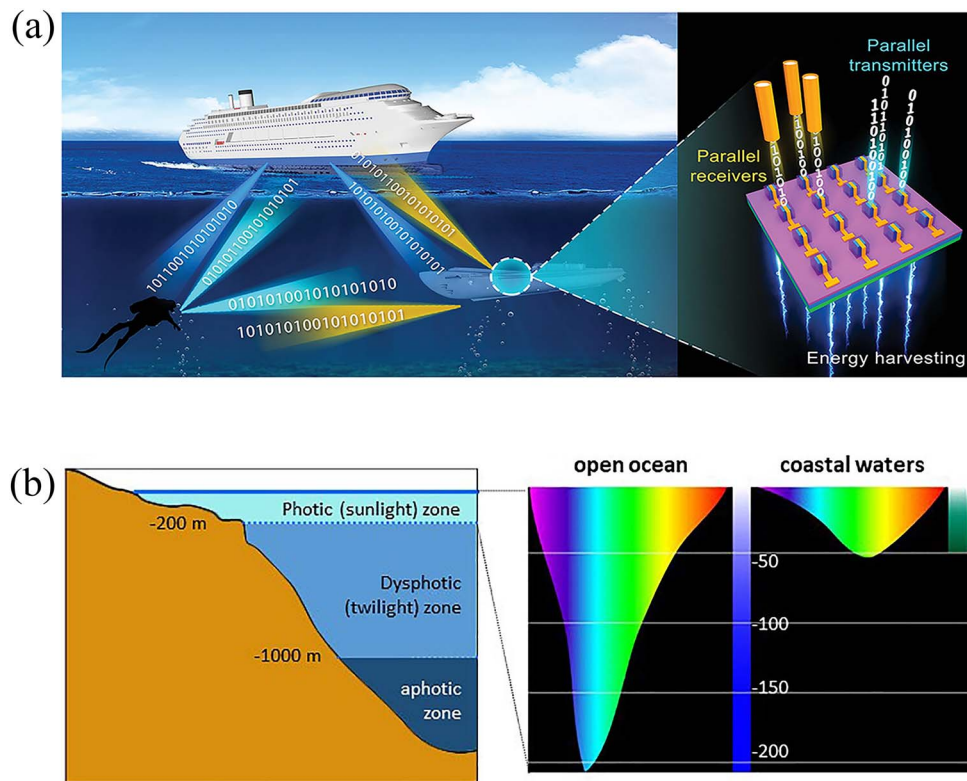
Fig. 2 (a) Schematic diagram of a duplex UWOC system based on a LED array. Reproduced with permission from ref. 25. Copyright 2021, WILEY-VCH. (b) Penetration of light into the water column and illustration of the depth at which different colours penetrate ocean waters. Reproduced with permission from ref. 29. Copyright 2020, Frontiers.

use of analogue equalizers at the transmitter and receiver sides, the implementation of a blue-light bandpass filter at the receiver to eliminate the phosphorescent component, and the adoption of different modulation schemes such as quadrature amplitude modulation (QAM) and orthogonal frequency division multiplexing (OFDM).[20,21] Minh *et al.* successfully increased the bandwidth of a WLED to 50 MHz using an analogue equalizer, achieving a transmission rate of 100 Mbps.[22] Additionally, reducing the active LED area reduces device capacitance and increases the bias current density, thereby widening the modulation bandwidth.[23] This principle has led to the development of Micro-LED arrays.[24] Tian *et al.* documented a peak modulation bandwidth of 251.3 MHz and a data rate of 660 Mbps using green micro-LEDs in a duplex UWOC system.[25] Xu *et al.* proposed a LED-to-LED UWOC system based on series of connected micro-LED arrays. Zhang *et al.* designed a real-time UWOC system with four blue LEDs, achieving a maximum communication range of 25.4 m at 80 Mbps.[26] The normalized detection bandwidth obtained demonstrates that increasing the number of LEDs improves the performance and practicability of LED UWOC systems.

Another critical aspect to consider in UWOC is the influence of water depth on the spectral components and light intensity. Purple light with a wavelength below 360 nm and red light with a wavelength above 600 nm are rapidly absorbed by surface water, while blue-green light tends to penetrate much deeper, reaching up to a level of 200 m in the open ocean (Fig. 2b).[27–29]

This penetration may be adequate with respect to the distance requirement of UWOC data transmissions. A shore-to-underwater VLC system has been proposed by Chung *et al.*, taking into account the varying light penetrability in onshore and underwater environments.[30] The signal was transmitted from the lighthouse equipped with WLEDs and received by a beacon that relayed the signal to the undersea receivers comprised of positive-intrinsic-negative photodiodes (PDs). The signal was then fed to a green LED driver and transmitted through an undersea optical channel. This study demonstrated that an underwater data rate transmission of up to 1 Gbps can be achieved over shorter distances, surpassing the performance of WLED-based VLC systems. Therefore, the development of blue or green LED devices specifically tailored for underwater applications holds great promise for advancing UWOC technology.

Nowadays, UWOC has emerged as a unique technology enabling high-speed data and moderate-distance communications in undersea environments. Numerous applications that demand high data transmission rates, such as real-time video transmission and remote-operated vessel control, stand to benefit significantly from UWOC. To date, UWOC has heralded the advent of a 100 meter high-speed connectivity paradigm. Besides, UWOC transmission of 40 m/1 Gbps and 100 m/1 Gbps levels can be achieved using a wide-bandwidth photomultiplier tube (PMT) and a high-bandwidth single-photon counter, respectively.[31,32] Future research direction in UWOC will focus

on LED-based transmission, optimal coding, and modulation technologies, aiming to achieve high-speed, long-distance, and real-time communications. In practical applications, the intricacies of the subaquatic milieu, including the presence of marine plankton, hydrodynamic perturbations, and other disruptive elements, exert a clear influence on the integrity and performance of UWOC systems.[33] Specifically, mobile UWOC network systems must account for the architectural parameters of subaquatic optical systems, including the emission divergence angle, the reception field of view, and other pivotal determinants.

2.2 Marine fishery

2.2.1 Fish-attracting lamps. Light plays a vital role in the environment inhabited by marine organisms. Spectral components, light intensity, and photoperiod are key factors that influence their behaviour. Phototaxis, the movement of a living organism in response to the presence of light and/or to its direction, either towards the light (positive) or away from the light (negative), plays a crucial role in several biological phenomena, including reproduction and diet.[34,35] The diversity of phototaxis behaviours observed in marine organisms is related to variations in their photosensitivity, as shown in Table 1, as well as to light penetration depth.[36] Aquatic species living in shallow water such as *Asparagopsis taxiformis*, *Cherax quadricarinatus*, and *Crassostrea gigas* show moderately positive phototaxis to red light.[35,37,38] As shown in Fig. 2b, blue-green light tends to penetrate much deeper in water than other wavelengths. Therefore, strong positive phototaxis of most deep-sea organisms occurs under blue or green light. For centuries, artificial light for the night-time purse seining has emerged as a highly effective and successful method for manipulating the movement of commercially valuable fishes like squid, hairtail, anchovy, and other phototactic fishes.[3] Among light sources, pc-LED devices have gained considerable attraction due to their exceptional energy efficiency and easy colour tuning.[39,40]

Most of the research in this area has focused on evaluating the influence of pc-LED emitting different colours and intensities on fish-attracting efficiency. For instance, a study revealed that Japanese flying squids exhibit heightened sensitivity to blue and green light, with a peak spectral sensitivity at 482 nm.[41] Additionally, research demonstrated the successful application of combined white LED and blue LED configurations in attracting squids, both in controlled tank settings and open-sea

trials.[42] Furthermore, researchers have recognized the variations in phototaxis behaviour across different life stages. Juvenile fish typically exhibit stronger phototaxis responses compared to their adult counterparts. This implies that employing full-spectrum white light or inappropriate light intensities can lead to the undesirable capture of predominantly juvenile fish, potentially jeopardizing the ecosystem and compromising fishing efficiency.[43] Extensive research has sought to unravel the phototactic patterns of various commercially important fish species using LED as fishing light sources.[44–46] Despite advances in understanding phototactic behaviour, the connection between phosphors design in pc-LEDs and fish-attracting lamp efficacy remains elusive and understudied. This gap persists due to the limited understanding of the underlying mechanisms governing light-mediated attraction and repulsion in marine organisms.[36] Besides, the application of commercial fish-attracting lamps is limited by many factors, such as light pollution caused by excessive power of flashlights, mismatch between lighting systems and flashboats, *etc.* However, recent discoveries offer promising solutions; for instance, Liu *et al.* successfully synthesized a novel phosphor material with multi-colour tuneable emission covering the spectral sensitivity range of most marine fish species.[47] Further elucidating the fundamental reasons behind variations in photosensitivity holds potential for optimizing fish-attracting lamps. Such progress paves the way for more sustainable and productive fishing practices, characterized by enhanced energy efficiency and reduced ecological impact.

2.2.2 Aquaculture in marine ranching systems. Marine ranches, featuring artificial aquaculture platforms, represent a modern approach to promoting sustainable fishery development.[48] Pc-LEDs offer a unique opportunity to tailor the lighting environment within these ranches, potentially enhancing the quality and yield of cultured aquatic species. The spectral preferences of aquatic organisms significantly impact their optimal growth conditions. For instance, several cultured fish species, like clownfish *Amphiprion clarkia*,[49] barfin flounder *Verasper moseri*,[50] or goldfish *Carassius auratus*[51] exhibit phototaxis towards short-wavelength light, while others, such as *Perca fluviatilis*,[52] *Anguilla marmorata*,[53] *Silurus meridionalis*, or *Wallago attu*[54] prefer red light. These variations are likely associated with differences in visual pigments and the spectral sensitivity of active substances within their bodies. Apart from the own factors of cultured fish species above, specific light can

Table 1 Visual sensitivity of various aquatic species

	Cephalopod	Fish	Crustacean
Visual structure	Single eye	Single eye	Compound eye
Identifiable light colour	Colour blindness	Wide range	Blue-green (440–570 nm), purple-ultraviolet (360–440 nm)
Optimum colour or wavelength	Blue, green, and white	Blue-green: *cyprinus carpio*, *carassius cuvieri*, *amphiprion clarkii* Red: *verasper moseri perca fluviatilis*, *silurus meridionalis*, *anguilla marmorata*, *wallago attu*	480–500 nm (deep sea), 510–525 nm (coastal) green light (530 nm), broadband white light

positively influence the formation of the microorganism community and the water quality by affecting the photosynthesis and nitrification process, reflecting on the growth performance of the cultured fish species.[55] Beyond colour, both light intensity and photoperiod (the period during which an organism is illuminated) significantly affect the growth and survival of cultured species. Wijgerde *et al.* demonstrated a positive correlation between the specific growth rate of coral and light irradiance.[56] Similarly, Dou *et al.* observed an improved survival and development of *Portunus trituberculatus* larvae under high-intensity full-spectrum LED lighting.[57] Interestingly, as reported by Ye *et al.*, *Micropterus salmoides* exhibits optimal growth under 24 h-continuous LED illumination with low-light intensity.[58] Additionally, varying photoperiods have been shown to promote growth in different development stages of *Takifugu rubripes* larvae.[59] Previous studies have shown that organisms can achieve better growth conditions under the optimum combination of illumination conditions. For example, Kim *et al.* found that compared to conventional WLED, green-emitting LED devices with an extended photoperiod can positively affect the production of pituitary and sex hormones, and reduce the stress response in *S. japonicus*.[60]

Despite significant progress in understanding the impact of light on aquaculture, further research is needed to elucidate the precise mechanisms governing these responses. Additionally, the design of pc-LED systems for marine ranches faces challenges associated with the long-term lighting requirements and the harsh environment characterized by high humidity and salinity. Continued advancements in pc-LED technology and a deeper understanding of light-mediated responses in various species hold great potential for optimizing the productivity and sustainability of marine ranches.

By leveraging the versatility of pc-LEDs, marine ranches can provide customized lighting environments for diverse aquaculture species. Tailoring light colour, intensity, and photoperiod based on the specific needs of each species offers a promising avenue for enhancing growth, development, and

ultimately, profitability. Continued research efforts dedicated to unravelling the intricacies of light-mediated responses in aquatic organisms, coupled with further technological advancements in pc-LEDs, are paving the way for sustainable and efficient aquaculture.

3 Developing phosphors for pc-LEDs in marine environments

Existing pc-LED devices are primarily designed for terrestrial applications and often exhibit limitations such as low energy efficiency and short lifespans under marine temperature and humidity conditions. Additionally, their broad emission bands hinder precise characterization of the impact of specific light on marine organisms. Therefore, pc-LEDs with tailored light colours and enhanced stability are crucial for effective deployment in practical marine applications. This review focuses on the role of phosphors, the key luminescent components in pc-LEDs, in addressing these critical challenges. By exploiting the tunability of rare-earth and transition metal ions, strategies for optimizing phosphor properties can be designed that meet the specific demands of the marine environment.

Phosphors dictate the optical properties of LEDs, such as luminous efficiency, colour temperature and colour rendering index (CRI). They are typically composed of host materials and activators; the former often include silicates, phosphates, aluminates, borates, perovskites, and nitrogen oxides, and the latter often include Ce^{3+}, Eu^{2+}, Bi^{3+}, Ln^{3+} (Ln = Sm, Eu, Tb, Dy, ...) or other transition metal ions. A large library of inorganic phosphors with specific emission colours has been developed and implemented in pc-LEDs, demonstrating high quantum efficiency at room temperature (Table 2). Notably, the inherent tunability of doping ions provides a powerful tool for manipulating the photoluminescent (PL) properties of phosphors. Several strategies can be employed to achieve the desired characteristics for marine applications, including colour tuning and stability enhancement.

Table 2 Selected rare-earth doped visible light emitting phosphors

Colour	Matrix	Doped activator	Excitation maximum (nm)	Emission maximum (nm)	Ref.
Red	$M_2Si_5N_8$ (M = Ca, Sr, Ba)	Eu^{2+}	450	623 (Ca)	61 and 62
				640 (Sr)	
				650 (Ba)	
	$SrLiAl_3N_4$	Eu^{2+}	440	650	63
	K_2SiF_6	Mn^{4+}	450	630	64
	$CaAlSiN_3$	Eu^{2+}	450	650	65
Yellow	$Y_3Al_5O_{12}$	Ce^{3+}	460	560	66
	$Sr[Li_{2.5}Al_{1.5}O_3N]$	Tb^{3+}	460	578	67
Green	$NaK_2Li[Li_3SiO_4]_4$	Eu^{2+}	450	528	68
	β-SiAlON	Eu^{2+}	325	540, 529	69
	$Lu_3Al_5O_{12}$	Ce^{3+}	460	530	70
	Ba_2SiO_4	Eu^{2+}	395	511	71
Blue	$BaMgAl_{10}O_{17}$	Eu^{2+}	254	450	72
	$Ca_4SnGe_3O_{12}$	Bi^{3+}	383	442	73
	$K_2SrBa(PO_4)_2$	Eu^{2+}	330	425	74
	$Ba_3Y_2B_6O_{15}$	Ce^{3+}	365	446	75

3.1 Blue-green phosphors with hight colour purity

Marine environment presents a unique and challenging frontier for pc-LED applications. The inherent attenuation of light in water necessitates the use of wavelengths with enhanced penetration, such as blue-green light (440–570 nm). Furthermore, the various photobiological responses of marine organisms highlight the importance of precise light control, achievable through narrow-band emission of phosphors. A series of narrow-band blue or green emitting phosphors have been developed for the backlighting of display, and these phosphors meet the colour requirements of the marine field.[76–81] This section introduces such blue- or green-emitting phosphors, as well as strategies to improve their colour purity.

For green-emitting phosphors, β-SiAlON: Eu^{2+} has dominated commercial applications for the past decade. Xie *et al.* reported Eu^{2+}-doped β-SiAlON ($Si_{5.6}Al_{0.4}O_{0.4}N_{7.6}$) phosphors with a strong response to excitation in the ultraviolet (UV) region and blue regions, and a peak emission at 535 nm (Fig. 3a).[82] However, β-SiAlON phosphors show broadband emission in a range from 525 to 540 nm, ultimately failing to meet the best emission range for marine applications. Besides, high-temperature synthesis with nitrogen oxide restricts further development. In contrast, UCr_4C_4-type compounds, $M(A, B)_4X_4$, emerge as more promising candidates for Eu^{2+}-doped commercial narrow-band phosphors (M is an alkali metal ion or alkaline earth metal ion, A and B are coordinated metal ions, X is oxygen or nitrogen ions). The corner-sharing and edge-sharing connections between $[AX_4]$ and $[BX_4]$ tetrahedra create a highly condensed three-dimensional network achieving narrow-band emission when doped with Eu^{2+}. Xia *et al.* pioneered this approach with oxide-based $RbLi(Li_3SiO_4)_2$:Eu^{2+} (RLSO:Eu^{2+}) and $RbNa(Li_3SiO_4)_2$:Eu^{2+} (RNSO:Eu^{2+}).[83,84] Compared to β-SiAlON:Eu^{2+}, these phosphors exhibit narrower emission bands (RLSO:Eu^{2+}-λ_{em} = 530 nm, full width at half height FWHM = 42 nm; RNSO: Eu^{2+}-λ_{em} = 523 nm, FWHM = 41 nm) and more suitable emission peak positions (Fig. 3b). These phosphors showcase narrow-band emission with high internal quantum efficiency (IQE) and excellent thermal stability. However, the presence of a large amount of alkali metal cations renders them susceptible to hydrolysis, leading to poor moisture resistance. To address this, surface modification or structural regulation can be applied. The detailed strategies will be discussed in Section 3.4.

In addition to the Eu^{2+}-doped phosphors described above, inorganic luminescent materials doped with Tb^{3+} are promising for their potential to emit narrow-band green light at 544 nm. However, the challenge lies in the weak UV absorption of Tb^{3+} ions, which is due to the parity-forbidden nature of f–f electric-dipole transitions. A common solution to overcome this is co-doping with Ce^{3+} as a sensitizer to enhance Tb^{3+} excitation through energy transfer. Notable examples include the borates $Sr_2LiScB_4O_{10}$:Ce^{3+}, Tb^{3+}, $Ba_2Lu_5B_5O_{17}$:Ce^{3+}, Tb^{3+}, the silicates $Gd_{4.67}Si_3O_{13}$:Ce^{3+}, Tb^{3+}, the aluminates $Ca_2TbHf_2Al_3O_{12}$:Ce^{3+}, $CaYAlO_4$:Tb^{3+}, Ce^{3+}, and the phosphate $Na_3Tb(PO_4)_2$:Ce^{3+}.[85–90]
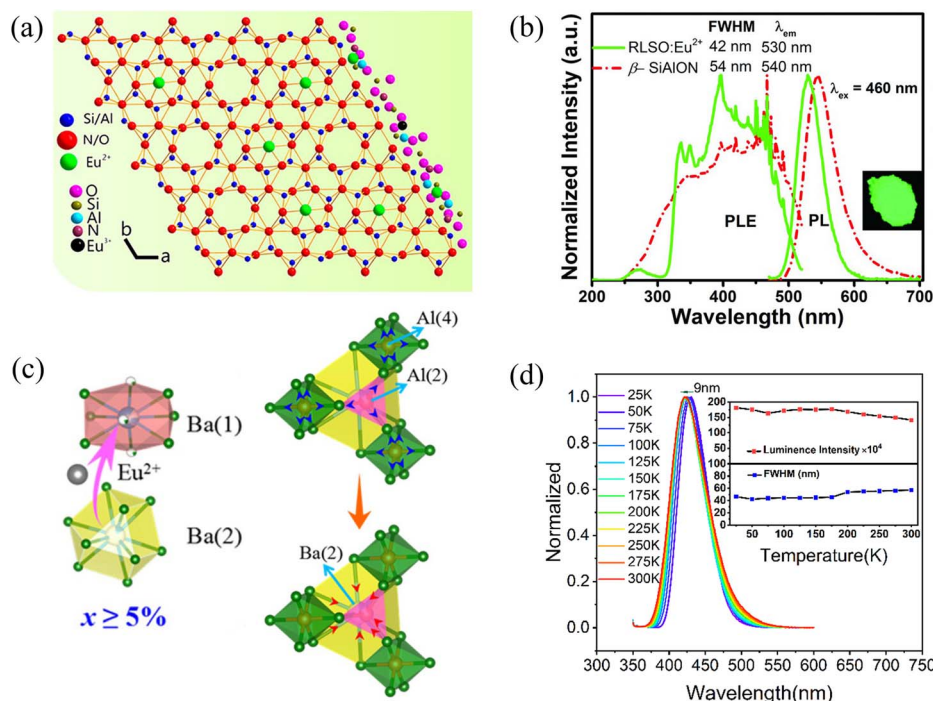

Fig. 3 (a) Crystal structure model of β-SiAlON. Reproduced with permission from ref. 82. Copyright 2018, ACS. (b) PLE and PL spectra of RLSO:8%Eu^{2+} and the commercial β-SiAlON:Eu^{2+} phosphors. The inset is a digital photograph of green RLSO:8%Eu^{2+} phosphor under 365 nm UV lamp illumination. Reproduced with permission from ref. 83. Copyright 2018, WILEY-VCH. (c) The proposed mechanism of the blue–shifted emission upon increasing Eu concentration (left) and the preferential site-occupancy of Eu^{2+} into Ba(1) and Ba(2) sites when $x \geq 5\%$ (right). Reproduced with permission from ref. 100. Copyright 2018, ACS. (d) PL spectra of the LaScO₃:Bi^{3+} sample under 344 nm excitation. The inset shows the luminescence intensity and FWHM from 25 K to 300 K. Reproduced with permission from ref. 107. Copyright 2022, Elsevier.

However, the 5d orbitals of Ce^{3+} extend beyond the electron shell, making it highly sensitive to environmental perturbations. This sensitivity leads to a broad absorption band and a wide, tuneable emission spectrum.[91] It is frequently reported that Ce^{3+}-activated phosphors tend to yield broadband emission, their FWHM values being usually larger than those of Eu^{2+}-doped phosphors. Therefore, most Ce^{3+}/Tb^{3+} co-doped phosphors have non-negligible Ce^{3+} emission in the UV and blue regions, reducing green colour purity. Besides that, divalent manganese (Mn^{2+}) also emerges as an alternative dopant for phosphors with high colour purity, due to the characteristic narrow-band green emission of Mn^{2+} in tetrahedral coordinating environments; on the other hand, in octahedral positions, Mn^{2+} emits in the red.[92,93] Xie et al. reported Mn^{2+} doped γ-aluminum oxynitride (γ-AlON) emitting a green band at 512 nm with FWHM of 32 nm under 445 nm excitation, surpassing β-SiAlON:Eu^{2+} in emission wavelength, bandwidth, and colour purity.[94] However, similarly to Tb^{3+}, Mn^{2+}-activated blue/green phosphors often suffer from low absorption or/and external quantum efficiency (EQE) due to parity forbidden electric-dipole d–d transitions.[95] Strategies like ion substitution and energy transfer can improve the external quantum efficiency, as seen in γ-AlON:Mn^{2+}, Mg^{2+} and γ-AlON:Mn^{2+}, Eu^{2+},[96,97] but there is still a problem of low internal quantum efficiency. It is noteworthy that the emission of Mn^{2+} is easily affected by the host crystal. Part of host materials with a strong charge transfer band absorption can be the ideal hosts for Mn^{2+}, and the optimal absorption peak has to match well with common n-UV or blue LED chips.[98] Accordingly, Wang et al. designed a series of gallate phosphors and successfully prepared NaGa$_{11-y}$Al$_y$O$_{17}$:Mn^{2+} (y = 0, 1, 2, 3) narrow-band green phosphor with an excellent external quantum efficiency (56.1%).[99]

Substrates for blue-emitting phosphors encompass a range of materials, including silicates, phosphates, aluminates, borates, and nitrogen oxides. Eu^{2+}, Ce^{3+}, or Bi^{3+} are commonly employed activator ions due to their favorable photoluminescent properties. Among commercially established blue phosphors, BaMgAl$_{10}$O$_{17}$:Eu^{2+} (BAM:Eu^{2+}) stands out for its high luminous efficiency.[72] However, drawbacks such as poor high-temperature stability and a broad emission band necessitate further development. In this regard, Lin et al. reported a promising alternative: the Eu^{2+}-doped BaAl$_{12}$O$_{19}$ (BAO) blue-emitting phosphor, exhibiting both high efficiency (IQE 90%) and colour purity (90%).[100] Due to the expansion of the Al polyhedron, the Ba(2) site becomes unsuitable for Eu^{2+} ions, favoring their preferential occupation of the single Ba(1) site, thereby leading to narrow-band emission and high thermal stability (Fig. 3c). Besides, several narrow-band blue-emitting phosphors have been reported, such as AELi$_2$[Be$_4$O$_6$]:Eu^{2+}(AE = Sr, Ba), RbNa$_3$(Li$_3$SiO$_4$)$_4$:Eu^{2+}, AEP$_8$N$_{14}$:Eu^{2+}(AE = Ca, Sr, Ba), Sr[B$_8$O$_{11}$(OH)$_4$]:Eu^{2+}.[101-104] Some, like UCr$_4$C$_4$-type phosphors, suffer from limited moisture stability, and others, like nitride phosphors, require harsh preparation conditions, hindering their commercial application. As the promising alternative, some perovskite-structure phosphors can be the particularly fascinating hosts for Eu^{2+}. Leng et al. reported a zero-thermal-quenching perovskite-like K$_2$BaPO$_4$F:1.5% Eu^{2+} phosphor with an ultra-narrow-band (FWHM = 25 nm) blue-emission and a high colour purity (99%), whose emission intensity can remain 91% of its pristine value after being exposed to the ambient atmosphere for 4 months.[105] Additionally, bismuth (Bi^{3+}) ions in various phosphor hosts can minimize spectral overlap and emit light across the ultraviolet to orange-red spectrum due to their 6p–6s transition. The ns^2-nsp transition of Bi^{3+} is more sensitive to local structure than 5d–4f electron transition of Eu^{2+}, posing a challenge in developing Bi^{3+}-activated, narrow-band emission phosphors.[73,106-109] To date, only a few such phosphors have been identified. For example, Wang et al. found that LaScO$_3$:Bi^{3+} perovskite-structure phosphors exhibit a notably narrow blue emission with high colour purity (92.26%) and internal quantum efficiency (98%) (Fig. 3d).[107] Lin et al. developed a Sr$_{10}$P$_6$O$_{25}$:Bi^{3+} phosphor with a narrow-band blue emission and good thermal stability (>82% at 150 °C), attributed to the small Stokes shift and introduction of Bi^{3+} into highly symmetric lattice sites.[108] Chen et al. reported that garnet-type Ca$_4$Hf(GeSi)$_3$O$_{12}$(CHGSO):xBi^{3+} phosphors show a narrow-band blue emission with a high colour purity of ∼95% under the excitation of n-UV LED chips.[109] The large band gap, high lattice rigidity and high symmetry of these phosphate, perovskite, and garnet hosts make them ideal for narrow-band emission of Bi^{3+} ions.

These studies provide valuable insights into the design criteria for phosphors with narrow-band emission and high colour purity. Generally, a rigid host crystal structure is crucial to minimize electron-phonon coupling, while a highly symmetrical coordination environment around the active ion helps reduce the influence of crystal-field splitting.[110-112] Furthermore, a single lattice site for doping minimizes spectral overlap from multiple luminescence centres. Regarding the activator ions mentioned above, most transition metals and trivalent rare earth ions show weak and narrow absorption in the UV region, while Bi^{3+}, Ce^{3+}/Eu^{2+} display broadband absorption due to the parity-allowed s–p and 4f–5d transitions, respectively. Furthermore, Ce^{3+} has a broader emission band than Eu^{2+}, attributed to the spin–orbit and crystal-field splitting of the ^2F ground state. Overall, Eu^{2+} and Bi^{3+} may be the dominant choices for developing phosphors with high colour purity. The design of these phosphors is a cornerstone of photoluminescence (PL) conversion, and the strategies for controlling the emission peak position are explored in the next section.

3.2 Wavelength tuning of blue-green emitting phosphors for marine pc-LED applications

Achieving high-colour-purity blue or green light in phosphors necessitates not only narrow emission half-peak widths but also precise control over the emission wavelength. This control depends on several factors, including the intricate interplay between the crystal structure and the coordination environment surrounding the luminescent centre. The reasons for the emission shift can be attributed to crystal-field splitting and electron cloud rearrangement effects. This section explores

some common methods for manipulating PL through targeted modifications.

One such method involves cation or anion substitution within the host lattice. This approach alters crucial parameters like bond lengths between the luminescent centre and its ligands, the coordination polyhedron volume, and consequently, the crystal-field strength around the centre. Such alterations directly influence the phosphor's emission spectrum. For instance, in the $Ca_{9-x}Sr_xLiGd_{2/3}(PO_4)_7$:$Eu^{2+}$ system, the emission wavelength red-shifts from 485 nm to 535 nm because of Ca^{2+} ions being replaced by Sr^{2+} ions, attributed to crystal-field splitting and energy transfer between cation sites (Fig. 4a).[113] Also, an obvious blue shift of the emission bands of Gd_3TaO_7:Bi^{3+} (λ_{em} = 505 nm) can be detected upon cation substitution, varying to 493 nm for Gd_2YTaO_7:Bi^{3+}, 484 nm for Gd_2LuTaO_7:Bi^{3+} and 471 nm for Gd_2LaTaO_7:Bi^{3+}.[114] Similar effects have been observed for anion substitution, for instance in $Sr_2Ba(AlO_4F)_{1-x}(SiO_5)_x$: Ce^{3+} phosphors.[115] Beyond single substitutions, a more versatile approach known as chemical unit co-substitution involves the simultaneous replacement of multiple atomic units within the host. This strategy offers increased control over luminescence properties. For example, Xia et al. successfully tuned the emission colour from green to blue in $Ca_2(Al_{1-x}Mg_x)(Al_{1-x}Si_{1+x})O_7$:$Eu^{2+}$ phosphors by replacing the $[Al^{3+}–Al^{3+}]$ unit with $[Mg^{2+}–Si^{4+}]$ (Fig. 4b).[116] In another case, Zhang et al. used chemical unit co-substitution in the lutetium aluminium garnet (LuAG) host, replacing LuO_8/AlO_4 units with SrO_8/SiO_4, to develop the efficient and thermally stable green phosphor $Lu_2SrAl_4SiO_{12}$:Ce^{3+} (LSAS:Ce^{3+}), which emits a blue-shifted emission peaking at 514 nm.[117] Similarly, Huang et al. observed a noticeable wavelength-tuning from 423 nm to 525 nm in the orthosilicate-orthophosphate structured phosphor $K_{1-x}(BaSr)_{(1+x)/2}(Si_xP_{1-x})O_4$:$Eu^{2+}$ ($0 \leq x \leq 1$) by employing a co-substitution strategy, which also improved the thermal stability due to an expanded bandgap and the introduced defect levels associated with the higher content of the phosphate anion group.[118]

Adjusting the doping concentration typically impacts luminescence intensity according to the concentration quenching mechanism. However, in certain phosphors, this adjustment

also affects the lattice site occupancy, leading to an emission wavelength shift.[119] For example, in the $Ba_{1-x}Eu_xSi_2O_2N_2$ system, increasing Eu^{2+} concentration red-shifts the emission peak from 490 nm to 500 nm.[120] This phenomenon stems from the shorter bond lengths formed between Eu^{2+} and its surrounding O/N ligands when it replaces larger Ba^{2+} ions. The resulting stronger crystal field weakens the energy of the 5d–4f transitions, leading to the observed red shift. Similar effects occur in $La_{3-x}Ce_xSi_6N_{11}$ and $Sr_{1-x}Eu_xSi_2O_2N_2$ phosphor systems.[121,122] When the host matrix possesses multiple available cation sites, manipulating the activator ion distribution across these sites, known as crystal-site engineering, offers another avenue for photoluminescence tuning. For example, Liang et al. demonstrated this approach in $CsKNa_2(Li_3SiO_4)_4$:Eu^{2+} phosphors. Introducing Li^+ ions controlled the migration of Eu^{2+} ions from K^+ sites to Na^+ sites, achieving spectral tuning from a cyan narrow band to a green narrow band (Fig. 4c).[76] Similarly, in $KSrScSi_2O_7$ phosphors, increasing the Eu^{2+} doping concentration triggers its migration from the Sr^{2+} sites to the Sc^{3+} sites through doping concentration-dependent crystal-site engineering, enabling tuneable photoluminescence from blue to cyan.[123] Further exemplifying this principle, $Ca_3La_{3(1-x)}Ce_{3x}(BO_3)_5$ phosphors exhibit different emission changes with increasing Ce^{3+} concentration.[124] Concretely, the emission intensity from the $Ce(2)^{3+}$ site steadily increases, while that from the $Ce(1)^{3+}$ site decreases. This behaviour arises from the preferential occupation of $Ce(2)^{3+}$ sites at higher doping concentrations. These examples show the effectiveness of various strategies, including cation/anion substitution, chemical unit co-substitution, and crystal-site engineering, in optimizing phosphor optical performances and achieving specific blue or green emission characteristics.

3.3 Thermal stability of phosphors for pc-LED

In practical applications of pc-LED devices, in addition to the specific requirements for emission colours and colour purity, the stability of luminescence must also be considered, with the most critical aspects being chemical and thermal stabilities.[106,125,126] In marine applications, the primary chemical
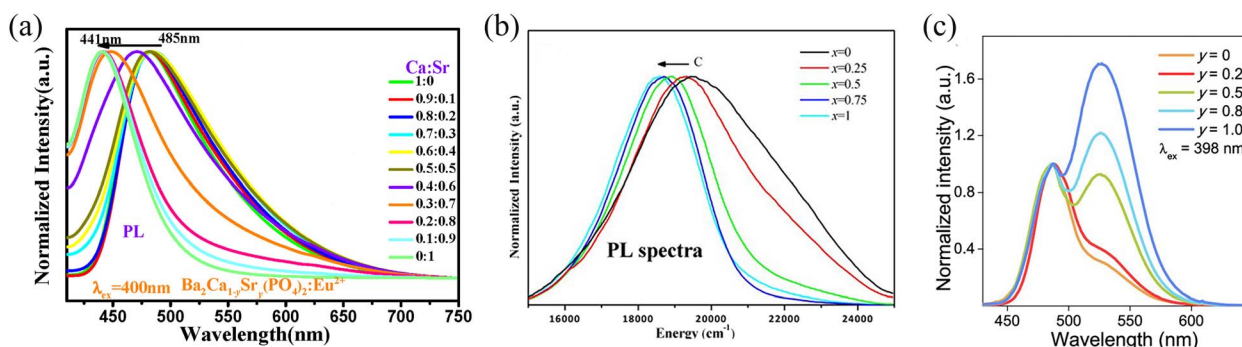

Fig. 4 (a) Normalized PL spectra of $Ba_2Ca_{1-y}Sr_y(PO_4)_2$:Eu^{2+}. Reproduced with permission from ref. 113. Copyright 2020, Elsevier. (b) PL spectra of the phosphors $Ca_{1.98}(Al_{1-x}Mg_x)(Al_{1-x}Si_{1+x})O_7$:$0.02Eu^{2+}$ (x = 0, 0.25, 0.5, 0.75, and 1) as a function of x. Reproduced with permission from ref. 116. Copyright 2015, ACS. (c) Normalized PL spectra of $CsKANa_{1.98-y}Li_y(Li_3SiO_4)_4$:$0.02Eu^{2+}$ ($0 \leq y \leq 1$). Reproduced with permission from ref. 76. Copyright 2019, ACS.

stability to consider is moisture resistance, which will be detailed in the following section.[127,128] While designing phosphors with high thermal stability is presented in this section. The thermal stability of PL in phosphors is evaluated by the thermal quenching (TQ) behaviour, which can be influenced by the electronic and/or crystal structures, structural rigidity, and chemical composition of the phosphors.[129] Within several years, many efforts have been devoted to designing anti-TQ phosphors, and the design strategies can be summarized as defect engineering, structural modulation, surface coating, and other strategies (*e.g.*, energy transfer, crystallinity enhancement, negative/zero thermal expansion, and glass technology).[112,130–134]

Defect engineering in phosphor materials refers to the deliberate introduction, manipulation, or control of defects within the structure to enhance or modify the optical properties. For phosphors with high thermal stability, energy levels associated with defects within the bandgap can inhibit TQ through energy transfer (ET) between the defect levels and luminescence centres. For example, the introduced Sr_{Ba} trap levels in $K_2Sr_{1.25}Ba_{0.75}(PO_4)_2:Eu^{2+}$ ($KS_{1.25}BP:Eu^{2+}$) phosphors enhance the thermal stability compared to the isomorphic K_2-$Ba_2(PO_4)_2:Eu^{2+}$ and $K_2Sr_2(PO_4)_2:Eu^{2+}$ phosphors (Fig. 5a).[135] Fig. 5b illustrates that these intentionally created point defects, mainly Sr_{Ba}, serve as electron-trapping centres. They store and transfer energy to the excitation band, leading to an emission increase, which counteracts the usual emission losses due to non-radiation (NR) transition at high temperatures. Some other

blue or green emitting phosphors such as $Sr_2SiO_4:Ce^{3+}/K^+$, $BaGa_2O_4:Bi^{3+}$, $Ba_4(CaLa)(PO_4)_3Cl:Eu^{2+}$, $Na_2MgAl_{10}O_{17}:Eu^{2+}$ also present high thermal stability *via* defect engineering.[136–139] Moreover, ET can occur not only between the defect levels and luminescence centres, but also in multiple luminescence centres through the interaction between two activators or electric multipole interactions.[140] Sensitizers can efficiently absorb UV/n-UV light and transfer energy to other luminescent centres, significantly enhancing the PL thermal stability of activators. In addition, PL thermal stability of luminescence centres can be enhanced by crystallinity improvement through adding flux during synthesis process of phosphors. Zhang *et al.* added a flux of K_2CO_3 into $K_3YSi_2O_7:Eu$ phosphors to improve the crystallinity and hinder the NR quenching process, so that integral intensity at 200 °C and quantum yield of the optimal sample can reach up to 200% enhancement compared to phosphors without flux adding.[141] The appropriate use of flux not only regulates the average size and shape of phosphor particles but also suppresses the impurity formation. This results in a pure phase with enhanced crystallinity and reduced surface defects, significantly impeding the non-radiative (NR) quenching process.

The preceding strategies are mainly based on the relationship between anti-TQ properties and the corresponding electronic structure of phosphor. Another aspect to be considered is the crystal structure. The TQ properties of phosphors can be strongly affected by structural modulations, which influence the local lattice environment around the luminescent ions. Concretely, a rigid structural framework such as β-K_2SO_4-, garnet-, and UCr_4C_4-type compound, can significantly reduce emission losses during the thermal processing (Fig. 5c).[142–144] Besides, chemical substitution can lead to enhanced structural rigidity and a concomitant decrease in lattice vibration frequency, thereby increasing the quenching temperature and moisture stability. This method and surface coating method will be introduced in Section 3.4 in more detail. Notably, several negative thermal expansion materials have been used as the matrix to develop anti-TQ phosphors. A 29-fold enhancement of green emission was observed in $Yb_2W_3O_{12}:Er^{3+}$ as the temperature rose from 30 to 300 °C, which may result from the increased efficiency in the accumulation of excitation energy due to the contraction and distortion of the host lattice (Fig. 5d).[145]
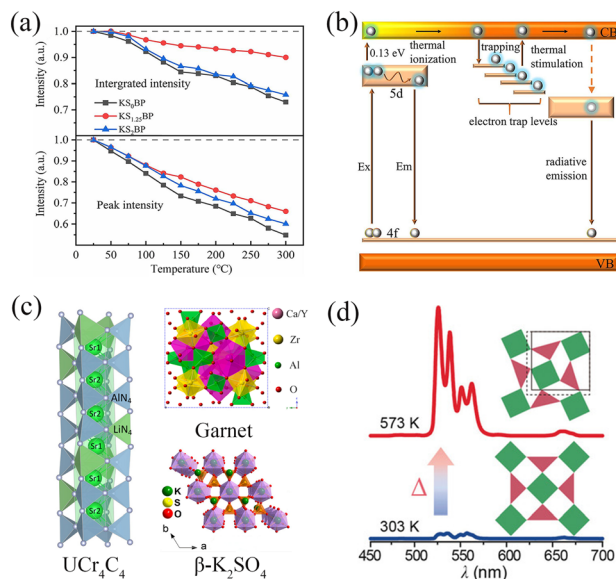

Fig. 5 (a) The emission retention of peak intensity and integrated intensity of $KS_xBP:Eu^{2+}$ ($x = 0, 1.25, 2$) as a function of temperature and (b) a suggested model for describing the mechanism of improved thermal stability. Reproduced with permission from ref. 135. Copyright 2022, Elsevier. (c) UCr_4C_4 structure, garnet structure, and β-K_2SO_4 structure model.[142–144] Reproduced with permission from ref. 142–144. Copyright 2023, ACS. Copyright 2023, Elsevier. Copyright 2018, ACS. (d) Thermal enhancement in Er^{3+}-doped orthorhombic $Yb_2W_3O_{12}$ by negative thermal expansion. Reproduced with permission from ref. 145. Copyright 2023, WILEY-VCH.

3.4 Moisture stability of phosphors for pc-LED

Considering the applications of pc-LEDs in the humid and salt-fog marine environment, it is necessary to combine structural regulation, surface modification, and other methods to further improve the luminescence stability of narrow-band blue-green phosphors. Fluoride and sulfide phosphors, for instance, exhibit strong hydrophilicity, readily undergoing hydrolysis or oxidation of the luminescent center or the inorganic matrix.[146,147] Besides, silicate- and nitride-based phosphors exhibit low emission efficiency under humid conditions.[63,148] These limitations hinder the application of pc-LED devices reliant on such phosphors in maritime environments. Extensive

research has identified various factors contributing to moisture-induced degradation, including structure decomposition,[149] luminescence centre oxidation,[150] and surface layer hydrolysis.[151] Consequently, phosphors for pc-LEDs often fall short of performance requirements in complex, humid atmospheres. To address this challenge, researchers have explored several strategies to enhance moisture resistance, including ionic substitution, surface modification, and the development of glass-ceramics phosphors, phosphor-in-glass (PiG) composites, and single-crystal phosphors.

3.4.1 Ionic substitution. Ionic substitution within the phosphor matrix presents a versatile approach to manipulate not only photoluminescence properties, including emission wavelength and bandwidth, but also crucial moisture resistance. This strategy is particularly well-documented for Mn^{4+}-doped phosphors, as Mn^{4+} readily transforms into $Mn(OH)_4$ under humid conditions. In Mn^{4+}-activated fluoride hosts like $A_2XF_6:Mn^{4+}$ and $A_3YF_6:Mn^{4+}$ (A = NH_4, Cs, K, Na; X = Ti, Zr, Si, Ge; Y = Ga, Al), hydrolysis of the $[MnF_6]^{2-}$ group significantly compromises moisture stability. Cation substitution, such as Si^{4+}-doping in $K_2GeF_6:Mn^{4+}$, Li^+-doping in $Na_2SiF_6:Mn^{4+}$, and Nb^{5+}-doping in $K_2TiF_6:Mn^{4+}$, effectively suppress this hydrolysis.[152–154] Notably, Nb^{5+} incorporation significantly improves both moisture resistance and luminescence intensity in $K_2Ti_{0.949}Nb_{0.051}F_{6.051}:5.0\%Mn^{4+}$ (Fig. 6a). Another prevalent strategy involves introducing oxygen atoms into the host lattice, forming more stable $Mn^{4+}–O^-$ and $Mn^{4+}–O^{2-}$ bonds compared to $Mn^{4+}–F^-$ bond.[155] As illustrated in Fig. 6b, $K_2NbF_7:Mn^{4+}$ and $K_3(NbOF_5)(HF_2):Mn^{4+}$ exhibit distinct luminescence declines after 360 min of water immersion. This approach also holds promise for enhancing moisture resistance in phosphors with other luminescent centers, as demonstrated by the increased moisture stability of $Sr_3AlO_4F:Ce^{3+}$ compared to the iso-structural $Sr_2BaAlO_4F:Ce^{3+}$ phosphors.[156] Liao et al. further reported that substituting Rb^+ with Na^+ noticeably increased the integrated PL intensity of $R_3NLSO:8\%Eu^{2+}$ compared to $R_4LSO:8\%Eu^{2+}$ phosphor after one hour in humid conditions (Fig. 6c).[157] Notably, ionic substitution in halide perovskite-based phosphors can minimize defect density and promote

radiative recombination, leading to enhanced stability. Previous studies have shown that sodium alloying followed by Bi^{3+} doping elevates the diffusion barrier of V_{Cl}^+ in cubic $Cs_2AgInCl_6$ perovskite, thereby improving its moisture stability.[158] The $Cs_2Ag_{0.7}Na_{0.3}InCl_6:Bi^+$ sample, for instance, retains ~98% of its initial PL intensity after desiccation. Overall, ionic substitution offers a versatile approach for tailoring phosphor structural units, promoting exciton recombination rate, and enhancing crystal structural stability, leading to intense and moisture-resistant light emissions. This strategy is ideal for optimizing the narrow-band-emission UCr_4C_4-type and aluminium oxynitride phosphors mentioned previously.

3.4.2 Surface modification. While structural and composition design offer promising avenues for improving moisture stability, surface modification presents a simpler and more versatile approach. This technique involves altering the phosphor particle surface through various strategies, including coating with heterogeneous or homogeneous materials, passivation treatment, and employing chemical bonding, precipitation reaction, or mechanochemistry.[159–162]

3.4.2.1 Protective coating layers. As mentioned previously, alkaline earth silicate and aluminate substrates are popular choices for blue-green phosphors due to their suitable properties for pc-LEDs. However, their instability in water hinders their commercial viability in marine environments. To address this problem, protective homogeneous coating layers using materials like SiO_2, Al_2O_3, and MgO, organo-silicone, resin, polyurethane, oleic acid (OA), and alkyl phosphates can be deposited.[163,164] For instance, Yoo et al. demonstrated plasma coating of $SrAl_2O_4:Eu^{2+}$, Dy^{3+} (SAO) with silane-based material, confirming no detrimental effects on the luminescence performance. This plasma-coated SAO phosphor retained over 50% of its initial luminescence intensity after 48 h in water. Ma et al. found that after being soaked in deionized water, the luminescence intensity of $K_2SiF_6:Mn^{4+}$ phosphors using oleylamine (OAm) as an organic coating layer remained 85.2% of its initial value, while that of non-coated KSFM decreased to 15.4%.[165] Xia et al. developed a $RLSO:Eu^{2+}$ phosphor with superior thermal stability but poor humidity resistance.[83] Heterogeneous protective layers, such as those obtained using atomic layer deposition (ALD), offer advantages like uniformity, densification, and precise control over layer thickness. By ALD strategy, Xia et al. created a dual-core-shell structure in $RLSO:Eu^{2+}@Al_2O_3@ODTMS$ (ODTMS is octadecyltrimethoxysilane), significantly enhancing water corrosion resistance (Fig. 7a).[166] However, these heterogeneous coatings exhibit long-term detachment issues under high temperatures and humidity. In contrast, the homogeneous core–shell approach offers better stability and reduces non-radiative transitions compared to heterogeneous coatings, and does not easily fall off in a high-humidity environment. Current reports on the moisture resistance of homogeneously coated core–shell phosphors are more common for Mn^{4+}-doped red fluoride phosphors. Chen et al. assembled a $KTF:Mn^{4+}@KTF$ core–shell phosphor via reverse cation exchange.[161] The KTF shell not only protects the $[MnF_6]^{2-}$ group inside the phosphor from hydrolysis, but, also, effectively cuts off energy migration to the surface layer,
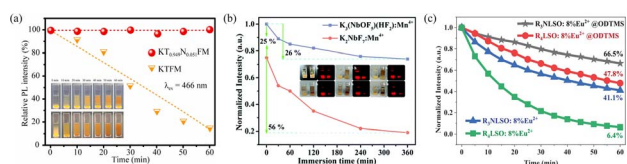
Fig. 6 (a) Relative emission intensity (λ_{ex} = 466 nm) and photographs of $K_2Ti_{0.949}Nb_{0.051}F_{6.051}:5.0\%Mn^{4+}$ (the upper illustration) and $K_2TiF_6:5.0\%Mn^{4+}$ (the inferior illustration) after immersion in deionized water for different times. Reproduced with permission from ref. 153. Copyright 2021, Elsevier. (b) Normalized emission intensity and photographs of $K_3(NbOF_5)(HF_2):Mn^{4+}$ and $K_2NbF_7:Mn^{4+}$ red phosphors at 630 nm after various immersion times. Reproduced with permission from ref. 155. Copyright 2019, the Royal Society of Chemistry. (c) Time-dependent normalized PL intensities of $R_3NLSO:8\%Eu^{2+}@ODTMS$, $R_4LSO:8\%Eu^{2+}@ODTMS$, $R_3NLSO:8\%Eu^{2+}$, and $R_4LSO:8\%Eu^{2+}$ immersed in water. Reproduced with permission from ref. 157. Copyright 2021, WILEY-VCH.
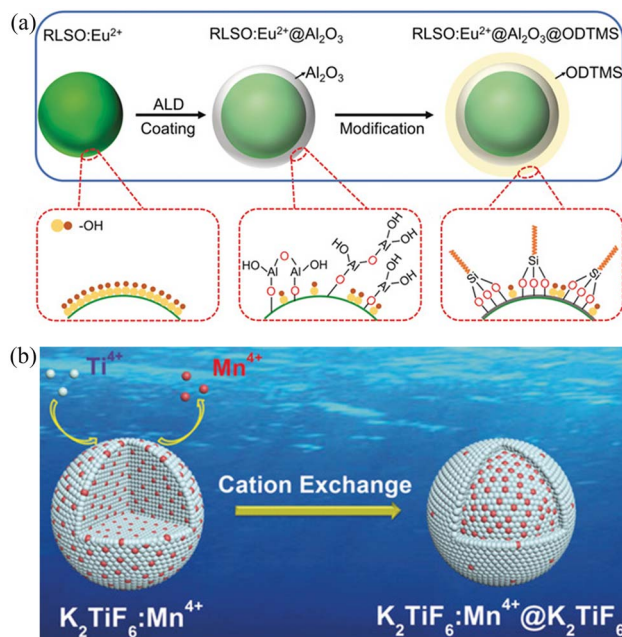
Fig. 7 (a) Schematic illustration of surface coating *via* atomic layer deposition (ALD) for the RLSO: Eu^{2+} phosphor and subsequent hydrophobic surface modification with ODTMS on RLSO:Eu^{2+}@Al_2O_3 surface. Reproduced with permission from ref. 166. Copyright 2020, WILEY-VCH. (b) Illustration of the construction of KTF: Mn^{4+}@KTF core−shell phosphor through a reverse cation-exchange strategy. Reproduced with permission from ref. 161. Copyright 2019, WILEY-VCH.

thereby increasing the luminous efficiency, especially for high-concentration phosphors (Fig. 7b).

3.4.2.2 Passivation treatment. Weak reducing agents like phosphoric acid,[167] H_2O_2,[168] oxalic acid,[169] and mandelic acid[170] can be used to form a surface passivation shell, reduce surface defects and improve chemical stability. This method offers advantages such as post-processing on existing phosphors or potential reduction of defects affecting ions like Mn^{4+} and Eu^{2+}. Li *et al.* demonstrated successful passivation of K_2SiF_6:Mn^{4+} with sodium sulfite, the phosphor maintaining 90.8% of its initial intensity after 6 h in water.[171] Ulteriorly, Chang *et al.* found that K_2SiF_6:Mn^{4+} phosphors maintained 95.2% of their emission intensity after immersing in deionized water for 6 h.[172] Reducing agent passivation is an environmentally friendly, cost-effective, and simple approach for enhancing moisture resistance while preserving the high luminous efficiency of pc-LED phosphors.

In summary, surface modification presents a versatile and effective approach for improving the moisture stability of phosphors, paving the way for their successful application in marine environments. Exploring and optimizing coating materials and passivation strategies is needed for further advancements in this field.

3.4.3 Other strategies. In practical applications, pc-LED devices are encapsulated into epoxy or silicone elastomers by combining the InGaN chip, phosphors, and encapsulants to fabricate the final device.[125] However, heat generated by

phosphors and excitation sources can discolour organic encapsulants, reducing luminous efficacy. To overcome this, inorganic materials like transparent ceramics or glass ceramics are realistic alternatives.[173,174] Phosphor-in-glass (PiG) technology disperses phosphors within an inorganic glass matrix, significantly enhancing stability towards water and oxygen.[175,176] This composite material retains the optical properties of the initial phosphors while offering superior moisture resistance compared to conventional surface modifications, as well as better transparency. Im *et al.* demonstrated this by fabricating $SrGa_2S_4$:Eu^{2+} PiG microcubes with improved thermal and moisture resistance.[177] Similarly, Zhang *et al.* embedded the $SrLiAl_3N_4$:Eu^{2+} phosphor in low-melting Sn–P–F–O glass, maintaining 80% of the initial luminous intensity.[178] Lei *et al.* even developed a blue light converter using a $SrLu_2O_4$:Ce^{3+}, Li^+, and F^- glass ceramics phosphor suitable for near-UV excitation (Fig. 8a).[179] Notably, PiG technology can also be applied to nanocrystals, further expanding its potential in pc-LED applications. For instance, Xu *et al.* synthesized Cs_2CuCl_4 glass ceramics showing stable blue emission even after 80 days in water.[180] Regarding their high stability and thermal conductivity, PiG films have been considered as suitable colour converters in the UWOC system. Xie *et al.* produced a laser-driven green light using blue laser diodes to excite the green-emitting β-Sialon PiG film.[181] The dominant wavelength of this green light, crucial for UWOC, can be adjusted between approximately 520–540 nm by controlling the phosphor content (around 60–80%) and film thickness (approximately 150–185 μm). This research also paves the way for pc-LED light sources in marine applications.
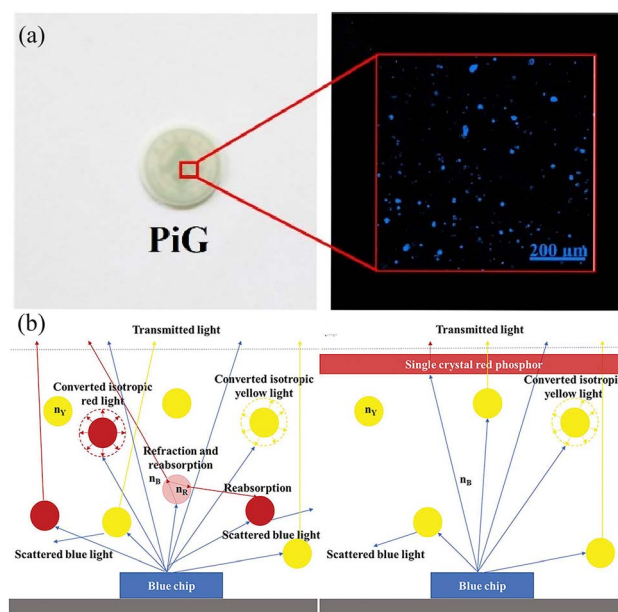

Fig. 8 (a) Digital picture and confocal laser scanning microscope image of PiG. Reproduced with permission from ref. 179. Copyright 2020, Elsevier. (b) Luminescence behaviors of powdery (left) and crystal phosphors (right) in WLEDs. Reproduced with permission from ref. 183. Copyright 2020, WILEY-VCH.

However, PiG and transparent ceramics face limitations in luminescence efficiency due to light scattering and reflection losses.[182] Single crystals, in contrast, offer advantages like superior moisture stability, reduced backscattering and minimized self-absorption due to fewer grain boundaries (Fig. 8b). This, along with minimized crystal defects, makes their luminescence less susceptible to ambient moisture.[183] Zhang *et al.* reported a micrometre-size $K_2SiF_6:Mn^{4+}$ (KSFM) single crystal with excellent moisture resistance obtained *via* saturated crystallization.[184] Wu *et al.* reported a $Cs_2TiF_6:Mn^{4+}$ (CTFM) single crystal with 98.7% internal quantum efficiency and strong moisture stability compared to the corresponding powder.[185] Notably, adding a homogeneous Cs_2TiF_6 shell using epitaxial growth further enhanced stability. While currently pc-LEDs are focused on red fluoride phosphors, similar materials can be developed for preparing blue-green phosphors, such as those with perovskite structures.

3.4.4 Comparing the various technologies proposed. Recent developments in moisture-resistant phosphors for pc-LEDs utilizing various technologies have been reviewed in the above sections and typical examples discussed. Ionic substitution, based on the influence of ion radius on structural stability, improves optical performance and moisture resistance but may introduce new defect states and alter the luminescence spectrum. Surface modification, the most widely used approach, enhances luminescence but when using organic protective shells, their thermal instability limits their applicability. Inorganic shells offer better thermal stability but pose challenges in controlling their formation due to higher sintering temperatures and potential interaction with the phosphor matrix. More research is needed to ensure composite materials retain the original phosphor's luminescence properties. Ultimately, strategies like PiG and single crystal phosphors offer better alternatives for all-inorganic pc-LED colour converters, eliminating the need for organic encapsulation. Developing highly efficient, chemically and thermally stable, and cost-effective phosphors for pc-LEDs remains an important but challenging task. Continued research in various modification and encapsulation technologies is crucial to achieving this goal.

4 Conclusions and outlook

As the field of solid-state pc-LED devices for marine applications continues to grow, innovative strategies to optimize and enhance the luminescence properties of phosphors offer exciting potential for future advancements. This review delves into the current applications of pc-LEDs in marine environments and explores strategies for developing suitable phosphors tailored to the unique demands of these environments. In underwater optical communications systems, pc-LED devices must meet stringent requirements of short response time, high bandwidth, and efficient information transfer. For marine fisheries, pc-LED devices that can precisely control light intensity, light colour, and photoperiod are crucial for optimizing the growth and well-being of specific species. To address these demands, previous research on narrow-band-emitting phosphors, photoluminescence

tuning, and environment-resistant phosphors provide valuable foundations for designing acceptable phosphors.

But despite the encouraging progress in phosphor discovery, several challenges and opportunities remain unexplored. These include the following aspects.

4.1 Distance and scope of optical beam transmission in UWOC

Water type, absorption, scattering, and other propagation losses significantly impact the range of the optical beam underwater. Blue-green wavelengths from pc-LED correspond to a low attenuation window and facilitate high-bandwidth communication over moderate distances.

4.2 Species-specific lighting needs in fisheries

Diverse aquatic species exhibit varying lighting needs and photosensitivity. The optimum light colour for most aquatic organisms lies within the blue-green spectral range. Strengthening research on improving the characteristics of underwater pc-LED light devices and on the photobiological effects of aquatic organisms will aid in developing lighting devices with emission wavelengths tailored to specific species.

4.3 Balancing narrow-band emission and environmental stability

While exploring phosphors with highly rigid and ordered structures for narrow-band blue or green emission is essential, achieving high environmental stability remains a challenge. Further research is warranted to develop phosphors that can simultaneously achieve both narrow-band emission and moisture resistance.

In conclusion, this review provides a comprehensive overview of the application directions and research progress in phosphor materials suitable for marine environments. By addressing the aforementioned challenges and opportunities, the development of marine pc-LED devices can be further advanced, paving the way for transformative applications in underwater communication, fisheries, and aquaculture.

Data availability

No primary research results, software or code have been included and no new data were generated or analysed as part of this review.

Author contributions

All the authors contributed to the literature search, writing, and editing of this review.

Conflicts of interest

There are no conflicts to declare.

Acknowledgements

References

1 L. Wang, Z. Qi, P. Liu, F. Hu, J. Li and Y. Wang, *J. Lightwave Technol.*, 2023, **41**, 5951–5957.

2 A. G. Nasser and M. A. A. Ali, *J. Opt. Commun.*, 2024, **44**, s1355–s1363.

3 C. Wang, Q. Chen, Z. Xiong, Z. Chen and R. Ye, *PLoS One*, 2024, **19**, e0301434.

4 M.-H. Wang, Y.-J. Hsieh, H.-H. Chang and Y.-S. Wang, *Aquaculture*, 2024, **578**, 740112.

5 M. Yu, C. Liu, L. Zhang and Y. Tang, *Front. Mar. Sci.*, 2022, **9**, 2439.

6 M.-H. Fang, Z. Bao, W.-T. Huang and R.-S. Liu, *Chem. Rev.*, 2022, **122**, 11474–11513.

7 N. D. Nhat, T. Van Dan, N. D. Q. Tram, N. Q. Lich, H. D. Phuc and N. N. Phuoc, *Aquacult. Fish.*, 2023, **8**, 551–557.

8 S. K. Gupta, J. P. Zuniga, M. Abdou, M. P. Thomas, M. D. A. Goonatilleke, B. S. Guiton and Y. Mao, *Chem. Eng. J.*, 2020, **379**, 122314.

9 B. Shao, J. Huo and H. You, *Adv. Opt. Mater.*, 2019, **7**, 1900319.

10 Z. Liu, Z. Li, T. Seto and Y. Wang, *Adv. Opt. Mater.*, 2023, **11**, 2300845.

11 C. Chen, M. Jin, J. Xiang, J. Zheng, P. Guo and C. Guo, *Ceram. Int.*, 2023, **49**, 25232–25239.

12 J. M. Ha, S. H. Hur, A. Pathak, J.-E. Jeong and H. Y. Woo, *NPG Asia Mater.*, 2021, **13**, 53.

13 B. A. Vijayalakshmi, S. Lekashri, M. Gomathi, R. Ashwini, B. Arunsundar and M. Nesasudha, *J. Opt.*, 2024, **2**, 1–10.

14 A. Elfikky, A. I. Boghdady, A. G. AbdElkader, E. E. Elsayed, K. W. Palitharathna, Z. Ali, M. Singh, S. A. H. Mohsan, M. Mahmoud and M. H. Aly, *Opt. Quantum Electron.*, 2024, **56**, 55.

15 L. Perera, P. Ranaweera, S. Kusaladharma, S. Wang and M. Liyanage, *IEEE Open J. Commun. Soc.*, 2024, **5**, 1753–1802.

16 G. Schirripa Spagnolo, L. Cozzella and F. Leccese, *Sensors*, 2020, **20**, 2261.

17 J. U. Rahman, S. Khan, V. Jain, A. Rajiv, S. Dasi, K. F. Fawy, P. K. Jindal and R. Sivaranjani, *Rev. Inorg. Chem.*, 2024, **5**, 44.

18 T. Lu, X. Lin, W. Guo, C.-C. Tu, S. Liu, C.-J. Lin, Z. Chen, H.-C. Kuo and T. Wu, *Opto-Electron. Sci.*, 2022, **1**, 220020–220024.

19 R. Wan, L. Wang, J. Huang, X. Yi, H.-C. Kuo and J. Li, *Adv. Photonics Res.*, 2021, **2**, 2100093.

20 M. Singh, S. A. Abd El-Mottaleb, A. Atieh and M. H. Aly, *Opt. Eng.*, 2024, **63**, 078105.

21 K. Bera, R. Parthiban and N. Karmakar, *IEEE Access*, 2023, **11**, 122833–122841.

22 H. Le Minh, D. O'Brien, G. Faulkner, L. Zeng, K. Lee, D. Jung, Y. Oh and E. T. Won, *IEEE Photonics Technol. Lett.*, 2009, **21**, 1063–1065.

23 D. Li, S. Liu, Z. Qian, Q. Liu, K. Zhou, D. Liu, S. Sheng, B. Sheng, F. Liu and Z. Chen, *Adv. Mater.*, 2022, **34**, 2109765.

24 W. C. Miao, F. H. Hsiao, Y. Sheng, T. Y. Lee, Y. H. Hong, C. W. Tsai, H. L. Chen, Z. Liu, C. L. Lin and R. J. Chung, *Adv. Opt. Mater.*, 2024, **12**, 2300112.

25 R. Lin, X. Liu, G. Zhou, Z. Qian, X. Cui and P. Tian, *Adv. Opt. Mater.*, 2021, **9**, 2002211.

26 M. Zhang and H. Zhou, *Sensors*, 2023, **23**, 7649.

27 D. R. Mishra, S. Narumalani, D. Rundquist and M. Lawson, *ISPRS J. Photogramm. Remote Sens.*, 2005, **60**, 48–64.

28 Z. Lee, C. Hu, S. Shang, K. Du, M. Lewis, R. Arnone and R. Brewin, *J. Geophys. Res.:Oceans*, 2013, **118**, 4241–4255.

29 J. Falcón, A. Torriglia, D. Attia, F. Viénot, C. Gronfier, F. Behar-Cohen, C. Martinsons and D. Hicks, *Front. Neurosci.*, 2020, **14**, 1183.

30 A. R. Darlis, W. A. Cahyadi and Y.-H. Chung, *Wirel. Pers. Commun.*, 2018, **99**, 681–694.

31 K. Sun, B. Han, J. Yang, B. Li, B. Zhang, K. Liu and C. Li, *Photonics*, 2023, **10**, 596.

32 T. Shen, J. Guo, H. Liang, Y. Li, K. Li, Y. Dai and Y. Ai, *Photonics*, 2023, **10**, 1238.

33 J. Fu, K. Zhu, S. A. H. Mohsan and Y. Li, *J. Mar. Sci. Eng.*, 2023, **11**, 547.

34 G. Kreimer, K.-i. Wakabayashi, P. Hegemann and C. Dieckmann, *The Chlamydomonas Sourcebook*, 2023, vol. 3, pp. 391–419.

35 H.-J. Kim, S. Umino and G. Satuito, *Hydrobiologia*, 2024, **2**, 1–10.

36 K. Q. Nguyen and P. D. Winger, *Reviews in Fisheries Science & Aquaculture*, 2019, **27**, 106–126.

37 R. Torres, A. M. Campos, J. Goldman, I. Barrote, L. Mata and J. Silva, *J. Appl. Phycol.*, 2024, **36**, 627–637.

38 C. Huang, X. Nie, J. Wei, Y. Wang, K. Hong, X. Mu, C. Liu, Z. Chu, X. Zhu and L. Yu, *Aquacult. Res.*, 2024, **2024**, 8897473.

39 N. Yeh, P. Yeh, N. Shih, O. Byadgi and T. C. Cheng, *Renewable Sustainable Energy Rev.*, 2014, **32**, 611–618.

40 G. B. Nair, H. Swart and S. Dhoble, *Prog. Mater. Sci.*, 2020, **109**, 100622.

41 H. Matsui, G. Takayama and Y. Sakurai, *Fish. Sci.*, 2016, **82**, 303–309.

42 H. Jeong, S. Yoo, J. Lee and Y.-I. An, *Renewable Energy*, 2013, **54**, 101–104.

43 Y. Ina, Y. Sakakura, Y. Tanaka, T. Yamada, K. Kumon, T. Eba, H. Hashimoto, J. Konishi, T. Takashi and K. Gen, *Fish. Sci.*, 2017, **83**, 537–542.

44 D. A. Guggiana-Nilo and F. Engert, *Front. Behav. Neurosci.*, 2016, **10**, 160.

45 J. D. Karlsen, V. Melli and L. A. Krag, *ICES J. Mar. Sci.*, 2021, **78**, 2818–2829.

46 Y. Qi, C. Liu, G. Yuan, H. Guo, J. Näslund, Y. Wang, J. Ru, Y. Ou, X. Chai and X. Zhang, *Animals*, 2024, **14**, 1701.

47 S. Liu, D. Wen, R. Du, C. Jiang, J. Chen, J. Li, L. Zhou, M. S. Molokeev and M. Wu, *Adv. Opt. Mater.*, 2023, **11**, 2203151.

48 X. Zhang, D. Sun, X. Zhang and H. Yang, *Aquaculture*, 2021, **534**, 736339.

49 H. S. Shin, J. Lee and C. Y. Choi, *Fish. Sci.*, 2012, **78**, 549–556.

50 T. Yamanome, K. Mizusawa, E. I. Hasegawa and A. Takahashi, *J. Exp. Zool., Part A*, 2010, **311A**, 73–79.

51 S. M. Noureldin, A. M. Diab, A. S. Salah and R. A. Mohamed, *Aquaculture*, 2021, **538**, 736532.

52 A. B. Head and J. A. Malison, *J. World Maric. Soc.*, 2010, **31**, 73–80.

53 Y.-T. Lin, W.-C. Hung, Y.-F. Yeh, K-M. Lu, D.-H. Cherng and Y.-S. Han, *Zool. Stud.*, 2023, **62**, e28.

54 S. S. Giri, S. K. Sahoo, B. B. Sahu, A. K. Sahu and S. Ayyappan, *Aquaculture*, 2002, **213**, 151–161.

55 W. G. Reis, W. Wasielesky Jr, P. C. Abreu, H. Brandão and D. Krummenauer, *Aquaculture*, 2023, **563**, 738924.

56 T. Wijgerde, P. Henkemans and R. Osinga, *Aquaculture*, 2012, **344**, 188–193.

57 J. Dou, G. Zhang, C. Shi, C. Song, C. Mu, Y. Ye and C. Wang, *Aquacult. Eng.*, 2021, **93**, 102158.

58 L. Ye, Y. Zhang, J. Zhao, X. Zhao, J. Li and Z. Ye, *Trans. ASABE*, 2021, **64**, 997–1005.

59 H. Ma, P. Wei, X. Li, S. Liu, Y. Tian, Q. Zhang and Y. Liu, *Aquaculture*, 2021, **542**, 736840.

60 Y. J. Choi, S. G. N. R. Park, A.-H. Jo and J.-H. Kim, *Fishes*, 2023, **8**, 77.

61 P. F. Smet, K. Van den Eeckhout, A. J. J. Bos, E. van der Kolk and P. Dorenbos, *J. Lumin.*, 2012, **132**, 682–689.

62 C.-W. Yeh, W.-T. Chen, R.-S. Liu, S.-F. Hu, H.-S. Sheu, J.-M. Chen and H. T. Hintzen, *J. Am. Chem. Soc.*, 2012, **134**, 14108–14117.

63 P. Pust, V. Weiler, C. Hecht, A. Tuecks, A. S. Wochnik, A.-K. Henss, D. Wiechert, C. Scheu, P. J. Schmidt and W. Schnick, *Nat. Mater.*, 2014, **13**, 891–896.

64 A. Vanetsev, P. Põdder, M. Oja, N. M. Khaidukov, V. N. Makhov, V. Nagirnyi, I. Romet, S. Vielhauer, H. Mändar and M. Kirm, *J. Lumin.*, 2021, **239**, 118389.

65 K. Zhu, Z. Chen, H. Liu, X. Yi, Y. Wang, J. Chen, X. Yuan and G. Liu, *J. Alloys Compd.*, 2023, **946**, 169353.

66 X. Liu, Y. Zhu, Z. Cheng, Y. Wang, F. Tian, Z. Liu, W. Li, G. Zhou, J. Zou and D. Y. Kosyanov, *J. Am. Ceram. Soc.*, 2024, **107**, 1061–1069.

67 G. J. Hoerder, S. Peschke, K. Wurst, M. Seibald, D. Baumann, I. Stoll and H. Huppertz, *Inorg. Chem.*, 2019, **58**, 12146–12151.

68 M.-H. Fang, C. O. M. Mariano, K.-C. Chen, J.-C. Lin, Z. Bao, S. Mahlik, T. Lesniewski, K.-M. Lu, Y.-R. Lu and Y.-J. Wu, *Chem. Mater.*, 2021, **33**, 1893–1899.

69 Y. Gao, J. Iihama, D. Hamana, R. Iwasaki, S. Honda, T. Asaka, M. Kumari, T. Hayakawa, S. Bernard and P. Thomas, *Int. J. Appl. Ceram. Technol.*, 2023, **20**, 768–779.

70 A. Markovskyi, V. Gorbenko, T. Yokosawa, J. Will, E. Spiecker, M. Batentschuk, J. Elia, A. Fedorov, M. Pakuła and M. Kaczmarek, *J. Alloys Compd.*, 2022, **929**, 167159.

71 Y. Wang, P. P. Zhang, L. Luo, X. T. Chen, R. Guo and J. Y. Xu, *J. Lumin.*, 2021, **239**, 118317.

72 K. B. Kim, Y. I. Kim, H. G. Chun, T. Y. Cho, J. S. Jung and J. G. Kang, *Chem. Mater.*, 2002, **14**, 5045–5052.

73 W. Xia, F. Du, Q. Zhao, L. Du, Z. Leng and Z. Tang, *J. Lumin.*, 2025, **277**, 120896.

74 T. Yang, Z. Ma, S. Huang, T. Zhang, K. Zhao, L. Yin, Q. Gu and P. Cao, *J. Alloys Compd.*, 2022, **892**, 162066.

75 A. C. Duke, S. Hariyani and J. Brgoch, *Chem. Mater.*, 2018, **30**, 2668–2675.

76 W. Wang, M. Tao, Y. Liu, Y. Wei, G. Xing, P. Dang, J. Lin and G. Li, *Chem. Mater.*, 2019, **31**, 9200–9210.

77 Y. Zhu, Y. Liang, S. Liu, H. Li and J. Chen, *Adv. Opt. Mater.*, 2019, **7**, 1801419.

78 Z. Long, M. Liu, X.-g. Wu, K. Gu, G. Yang, Z. Chen, Y. Liu, R. Liu and H. Zhong, *Nat. Synth.*, 2023, **2**, 1–9.

79 T. Jansen, J. Gorobez, M. Kirm, M. Brik, S. Vielhauer, M. Oja, N. Khaidukov, V. Makhov and T. Jüstel, *ECS J. Solid State Sci. Technol.*, 2017, **7**, R3086.

80 X. Zhang, M.-H. Fang, Y.-T. Tsai, A. Lazarowska, S. Mahlik, T. Lesniewski, M. Grinberg, W. K. Pang, F. Pan and C. Liang, *Chem. Mater.*, 2017, **29**, 6781–6792.

81 L. Yang, S. Gai, H. Ding, D. Yang, L. Feng and P. Yang, *Adv. Opt. Mater.*, 2023, **11**, 2202382.

82 S. Li, L. Wang, D. Tang, Y. Cho, X. Liu, X. Zhou, L. Lu, L. Zhang, T. Takeda and N. Hirosaki, *Chem. Mater.*, 2018, **30**, 494–505.

83 M. Zhao, H. Liao, L. Ning, Q. Zhang, Q. Liu and Z. Xia, *Adv. Mater.*, 2018, **30**, 1802489.

84 M. Liao, Z. Mu, Q. Wang, X. Zhang, H. Dong, M. Wen and F. Wu, *J. Alloys Compd.*, 2020, **837**, 155084.

85 H. Chen and Y. Wang, *Inorg. Chem.*, 2019, **58**, 7440–7452.

86 Y. Xiao, Z. Hao, L. Zhang, X. Zhang, G.-H. Pan, H. Wu, H. Wu, Y. Luo and J. Zhang, *J. Mater. Chem. C*, 2018, **6**, 5984–5991.

87 Y. Jin, Q. Wang, H. Zhou, L. Zhang and J. Zhang, *Ceram. Int.*, 2016, **42**, 3309–3316.

88 L. Zhou, J. Hong, X. Li, J. Shi, P. A. Tanner, K. L. Wong and M. Wu, *Adv. Opt. Mater.*, 2020, **8**, 2000523.

89 W. Xiao, X. Liu, J. Zhang and J. Qiu, *Adv. Opt. Mater.*, 2019, **7**, 1801677.

90 S. Huang, L. Yu, K. Peng, Y. Zhao, J. Wang and M. Shang, *J. Am. Ceram. Soc.*, 2021, **104**, 5848–5858.

91 C. Dou, Z. Song and Q. Liu, *J. Mater. Chem. C*, 2024, **12**, 11209–11241.

92 B. Su, G. Zhou, J. Huang, E. Song, A. Nag and Z. Xia, *Laser Photonics Rev.*, 2021, **15**, 2000334.

93 R. Zhang, H. Xie, W. Liu, K. Zhan, H. Liu, Z. Tang and C. Yang, *ACS Appl. Mater. Interfaces*, 2023, **15**, 47238–47249.

94 L. Liu, L. Wang, C. Zhang, Y. Cho, B. Dierre, N. Hirosaki, T. Sekiguchi and R.-J. Xie, *Inorg. Chem.*, 2015, **54**, 5556–5565.

95 P. Dang, H. Lian and J. Lin, *Adv. Opt. Mater.*, 2022, **11**, 2202511.

96 R.-J. Xie, N. Hirosaki, X.-J. Liu, T. Takeda and H.-L. Li, *Appl. Phys. Lett.*, 2008, **92**, 201905.

97 A. D. Sontakke, A. J. Van Bunningen, F. T. Rabouw, S. Meijers and A. Meijerink, *J. Phys. Chem. C*, 2020, **124**, 13902–13911.

98 C. Zhan, H. Zhu, S. Liang, Y. Huang, Z. Wang and M. Hong, *Inorg. Chem. Front.*, 2024, **11**, 826–836.

99 G. Lu, Y. Wang, K. Ma, X. Chen, W. Geng, T. Liu, S. Xu, J. Zhang and B. Chen, *Ceram. Int.*, 2024, **50**, 16190–16200.

100 Y. Wei, L. Cao, L. Lv, G. Li, J. Hao, J. Gao, C. Su, C. C. Lin, H. S. Jang and P. Dang, *Chem. Mater.*, 2018, **30**, 2389–2399.

101 P. Strobel, C. Maak, V. Weiler, P. J. Schmidt and W. Schnick, *Angew. Chem., Int. Ed.*, 2018, **57**, 8739–8743.

102 H. Liao, M. Zhao, M. S. Molokeev, Q. Liu and Z. Xia, *Angew. Chem., Int. Ed.*, 2018, **57**, 11728–11731.

103 S. Wendl, L. Eisenburger, P. Strobel, D. Günther, J. P. Wright, P. J. Schmidt, O. Oeckler and W. Schnick, *Chem.–Eur. J.*, 2020, **26**, 7292–7298.

104 P. Liang, W.-L. Lian and Z.-H. Liu, *Chem. Commun.*, 2021, **57**, 3371–3374.

105 Z. Leng, D. Zhang, H. Bai, H. He, Q. Qing, J. Zhao and Z. Tang, *J. Mater. Chem. C*, 2021, **9**, 13722–13732.

106 J. Ding and Q. Wu, *Dalton Trans.*, 2024, **53**, 15403–15411.

107 H. Yang, P. Li, X. Fu, Z. Ye, X. Huo, Y. Wang, Q. Wu, H. Suo, L. Li and Z. Wang, *Mater. Today Chem.*, 2022, **26**, 101050.

108 P. Dang, W. Yang, Q. Zhang, D. Liu, H. Lian, G. Li and J. Lin, *Opt. Mater.:X*, 2022, **13**, 100136.

109 S. Piao, Y. Wang, G. Zhu, J. Zhang, X. Zhang, D. Wu, Y. Cao, X. Li and B. Chen, *J. Mater. Chem. C*, 2021, **9**, 14777–14787.

110 H. Dong, L.-D. Sun and C.-H. Yan, *J. Am. Chem. Soc.*, 2021, **143**, 20546–20561.

111 Z. Pan, V. Castaing, L. Yan, L. Zhang, C. Zhang, K. Shao, Y. Zheng, C. Duan, J. Liu and C. Richard, *J. Phys. Chem. C*, 2020, **124**, 8347–8358.

112 Q. Liu, P. Dang, G. Zhang, H. Lian, Z. Cheng, G. Li and J. Lin, *Chem. Mater.*, 2024, **36**, 1763–1772.

113 H. Zhu, Z. Wang, X. Zhang, D. Wang, J. Zhao, Y. Sun, Z. Yang and P. Li, *Ceram. Int.*, 2020, **46**, 25556–25567.

114 J. Ding, Z. An, Z. Wang, Y. Dai, W. Yu, J. Deng, Y. Lai, X. Huang and Q. Wu, *Chem. Eng. J.*, 2023, **477**, 147122.

115 K. A. Denault, N. C. George, S. R. Paden, S. Brinkley, A. A. Mikhailovsky, J. Neuefeind, S. P. DenBaars and R. Seshadri, *J. Mater. Chem.*, 2012, **22**, 18204–18213.

116 Z. Xia, C. Ma, M. S. Molokeev, Q. Liu, K. Rickert and K. R. Poeppelmeier, *J. Am. Chem. Soc.*, 2015, **137**, 12494–12497.

117 Y. Xiao, W. Xiao, L. Zhang, Z. Hao, G.-H. Pan, Y. Yang, X. Zhang and J. Zhang, *J. Mater. Chem. C*, 2018, **6**, 12159–12163.

118 T. Yang, T. Zhang, T. D. Christopher, S. Huang and P. Cao, *Ceram. Int.*, 2024, **50**, 13862–13870.

119 P. Dai, Q. Wang, M. Xiang, T.-M. Chen, X. Zhang, Y.-W. Chiang, T.-S. Chan and X. Wang, *Chem. Eng. J.*, 2020, **380**, 122508.

120 Y. Q. Li, A. Delsing, G. De With and H. Hintzen, *Chem. Mater.*, 2005, **17**, 3242–3248.

121 N. Kijima, T. Seto and N. Hirosaki, *ECS Trans.*, 2009, **25**, 247.

122 V. Bachmann, C. Ronda, O. Oeckler, W. Schnick and A. Meijerink, *Chem. Mater.*, 2009, **21**, 316–325.

123 S. Lai, M. Zhao, Y. Zhao, M. S. Molokeev and Z. Xia, *ACS Mater. Au*, 2022, **2**, 374–380.

124 C. Liu, H. Liang, X. Kuang, J. Zhong, S. Sun and Y. Tao, *Inorg. Chem.*, 2012, **51**, 8802–8809.

125 Y. Wei, Z. Cheng and J. Lin, *Chem. Soc. Rev.*, 2019, **48**, 310–350.

126 C. Zhang, T. Uchikoshi, T. Takeda and N. Hirosaki, *Phys. Chem. Chem. Phys.*, 2023, **25**, 24214–24233.

127 Y. Zhang, J. Ling, Y. Li, W. Xu, Y. Zhou and M. Hong, *J. Lumin.*, 2022, **247**, 118886.

128 M.-H. Liu, T.-T. Li and D. L. Zhang, *Mater. Res. Bull.*, 2022, **154**, 111944.

129 P. Dang, W. Wang, H. Lian, G. Li and J. Lin, *Adv. Opt. Mater.*, 2022, **10**, 2102287.

130 P. Dang, G. Li, X. Yun, Q. Zhang, D. Liu, H. Lian, M. Shang and J. Lin, *Light:Sci. Appl.*, 2021, **10**, 29.

131 W. Zhou, J. Fan, J. Luo, L. Lin, J. Zhou, J. Zhang, Z. Zhu and X. Zhang, *Inorg. Chem.*, 2022, **61**, 8767–8781.

132 T. Zheng, L. Luo, P. Du, S. Lis, U. R. Rodriguez-Mendoza, V. Lavin and M. Runowski, *Chem. Eng. J.*, 2022, **446**, 136839.

133 L. Cao, W. Li, B. Devakumar, N. Ma, X. Huang and A. F. Lee, *ACS Appl. Mater. Interfaces*, 2022, **14**, 5643–5652.

134 T. Zheng, L. Luo, P. Du, S. Lis, U. R. Rodriguez-Mendoza, V. Lavin, I. R. Martin and M. Runowski, *Chem. Eng. J.*, 2022, **443**, 136414.

135 T. Yang, T. Zhang, S. Huang, T. D. Christopher, Q. Gu, Y. Sui and P. Cao, *Chem. Eng. J.*, 2022, **435**, 133873.

136 K. Zhao, Z. Ma, L. Yin, B. Hui, H. Si, X. Tong, H. Tang, P. Cao and S. Huang, *Inorg. Chem. Front.*, 2023, **10**, 2314–2324.

137 Y. Xu, S. Yin, X. Wu, C. Zhong, X. Zhang, L. Zhou and H. You, *Ceram. Int.*, 2024, **50**, 1159–1165.

138 Q. Zong, D. Zhao, R. J. Zhang, L. Jia and S.-Y. Zhu, *Ceram. Int.*, 2023, **49**, 24794–24801.

139 H. Li, J. Cai, R. Pang, G. Liu, S. Zhang, L. Jiang, D. Li, C. Li, J. Feng and H. Zhang, *J. Mater. Chem. C*, 2019, **7**, 13088–13096.

140 X. Lv, R. Xiao, J. Liu, C. Yang, Y. Xin and N. Guo, *Inorg. Chem. Front.*, 2024, **11**, 1668–1682.

141 W. Zhou, Z. Sun, J. Luo, X. Zhang, Q. Pang and L. Zhou, *J. Alloys Compd.*, 2021, **854**, 157188.

142 J. Bouquiaux, S. Poncé, Y. Jia, A. Miglio, M. Mikami and X. Gonze, *Chem. Mater.*, 2023, **35**, 5353–5361.

143 M. Qu, Z. Pang, T. Li, Q. Liu, Y. Yang and X. Zhang, *Ceram. Int.*, 2023, **49**, 792–800.

144 J. Qiao, L. Ning, M. S. Molokeev, Y.-C. Chuang, Q. Liu and Z. Xia, *J. Am. Chem. Soc.*, 2018, **140**, 9730–9736.

145 H. Zou, X. Yang, B. Chen, Y. Du, B. Ren, X. Sun, X. Qiao, Q. Zhang and F. Wang, *Angew. Chem., Int. Ed.*, 2019, **58**, 17255–17259.

146 J. Tang, X. Zhang, S. Liao, Y. Zhu, Y. Han, H. Su, Z. Qiu, S. Lian and J. Zhang, *Adv. Opt. Mater.*, 2024, **16**, 2401811.

147 X. Wang, Z. Qiu, Y. Li, Q. Mi, W. Zhou, S. Ai, J. Xu, Y. Liu and S. Lian, *J. Mater. Chem. C*, 2019, **7**, 5931–5936.

148 H. Yunsheng, H. Jianhua, W. Zhuang, X. Huang and H. Huaqiang, *J. Rare Earths*, 2011, **29**, 911–914.

149 X. Zhong, D. Deng, T. Wang, Y. Li, Y. Yu, J. Qiang, S. Liao, Y. Huang and J. Long, *J. Lumin.*, 2022, **243**, 118643.

150 Y. H. Kim, P. Arunkumar, B. Y. Kim, S. Unithrattil, E. Kim, S.-H. Moon, J. Y. Hyun, K. H. Kim, D. Lee and J.-S. Lee, *Nat. Mater.*, 2017, **16**, 543–550.

151 B. Guo, M. Wen, H. Tang, S. Lishik, X. Fan, G. Zhang and J. Fan, *Laser Photonics Rev.*, 2024, **18**, 2300838.

152 T. Lang, T. Han, S. Fang, J. Wang, S. Cao, L. Peng, B. Liu, V. I. Korepanov and A. N. Yakovlev, *Chem. Eng. J.*, 2020, **380**, 122429.

153 J. Zhou, F. Liu, J. Li, B. Milićević, J. Yan, Z. Wu and M. Wu, *Opt. Mater.*, 2021, **117**, 111184.

154 X. Zhong, D. Deng, T. Wang, Y. Li, Y. Yu, J. Qiang, S. Liao, Y. Huang and J. Long, *Inorg. Chem.*, 2022, **61**, 5484–5494.

155 G. Pang, F. Hong, X. Liu, Y. Zhang, C. Zhang, T. Dong, Z. Fu, G. Liu, J. Wang, D. Li and X. Dong, *Dalton Trans.*, 2021, **50**, 17290–17300.

156 W. B. Im, N. George, J. Kurzman, S. Brinkley, A. Mikhailovsky, J. Hu, B. F. Chmelka, S. P. DenBaars and R. Seshadri, *Adv. Mater.*, 2011, **23**, 2300–2305.

157 M. Liao, Q. Wang, Q. Lin, M. Xiong, X. Zhang, H. Dong, Z. Lin, M. Wen, D. Zhu and Z. Mu, *Adv. Opt. Mater.*, 2021, **9**, 2100465.

158 S. Li, Z. Shi, F. Zhang, L. Wang, Z. Ma, D. Wu, D. Yang, X. Chen, Y. Tian and Y. Zhang, *ACS Appl. Mater. Interfaces*, 2020, **12**, 46330–46339.

159 Y. Jia, Y. Pan, Y. Li, L. Zhang, H. Lian and J. Lin, *Inorg. Chem.*, 2021, **60**, 231–238.

160 P. Balaz, M. Achimovicova, M. Balaz, P. Billik, Z. Cherkezova-Zheleva, J. Manuel Criado, F. Delogu, E. Dutkova, E. Gaffet, F. Jose Gotor, R. Kumar, I. Mitov, T. Rojac, M. Senna, A. Streletskii and K. Wieczorek-Ciurowa, *Chem. Soc. Rev.*, 2013, **42**, 7571–7637.

161 D. Huang, H. Zhu, Z. Deng, Q. Zou, H. Lu, X. Yi, W. Guo, C. Lu and X. Chen, *Angew. Chem., Int. Ed.*, 2019, **58**, 3843–3847.

162 J. Xiong, N. Liu, X. Hu, Y. Qi, W. Liu, J. Dai, Y. Zhang, Z. Dai, X. Zhang and Y. Huang, *Adv. Energy Mater.*, 2022, **12**, 2201787.

163 Y. Liu, H. Wang, D. Chen, L. Gao, X. Wang, X. Jian, C. Mu, X. Xu, Y. Zhao and L. Yin, *Ceram. Int.*, 2021, **47**, 3244–3251.

164 R. Li, X. Fang, J. Ren, B. Chen, X. Yuan, X. Pan, P. Zhang, L. Zhang, D. Tu and Z. Fang, *Nanoscale*, 2021, **13**, 12494–12504.

165 C. Chang, W. Ye, C. Zuo, Y. Li, Z. Wen, L. Guo, Y. Cao and C. Ma, *ACS Sustainable Chem. Eng.*, 2023, **11**, 15887–15897.

166 M. Zhao, K. Cao, M. Liu, J. Zhang, R. Chen, Q. Zhang and Z. Xia, *Angew. Chem., Int. Ed.*, 2020, **59**, 12938–12943.

167 Q. Zhou, L. Dolgov, A. M. Srivastava, L. Zhou, Z. Wang, J. Shi, M. D. Dramićanin, M. G. Brik and M. Wu, *J. Mater. Chem. C*, 2018, **6**, 2652–2671.

168 Y. Zhou, E. Song, T. Deng, Y. Wang, Z. Xia and Q. Zhang, *Adv. Mater. Interfaces*, 2019, **6**, 1802006.

169 H. Yu, B. Wang, X. Bu, Y.-g. Liu, J. Chen, Z. Huang and M. Fang, *Ceram. Int.*, 2020, **46**, 18281–18286.

170 D. Li, Y. Pan, X. Wei and J. Lin, *Chem. Eng. J.*, 2021, **420**, 127673.

171 J. Qiang, L. Wang, T. Wang, Y. Yu, D. Deng, C. Wu, S. Liao and S. Li, *Ceram. Int.*, 2022, **48**, 17253–17260.

172 Y. Yu, C. Jiang, G. Chang, S. Liao and R. Li, *J. Lumin.*, 2024, **270**, 120532.

173 R. Zhang, H. Lin, Y. Yu, D. Chen, J. Xu and Y. Wang, *Laser Photonics Rev.*, 2014, **8**, 158–164.

174 M. He, J. Jia, J. Zhao, X. Qiao, J. Du and X. Fan, *Ceram. Int.*, 2021, **47**, 2963–2980.

175 M. Xia, J. Luo, C. Chen, H. Liu and J. Tang, *Adv. Opt. Mater.*, 2019, **7**, 1900851.

176 B. Yang, F. Zheng, S. Mei, Z. Chen, Y. Xie, H. Dai, X. Wei, W. Zhang, F. Xie and J. Ju, *Appl. Surf. Sci.*, 2020, **512**, 145655.

177 Y. H. Kim, P. Arunkumar and W. B. Im, *Ceram. Int.*, 2015, **41**, 5200–5204.

178 Y. Zhang, X. Zhang, H. Zhang, J. Zhuang, C. Hu, Y. Liu, Z.-C. Wu, L. Ma, X. Wang and B. Lei, *J. Colloid Interface Sci.*, 2019, **545**, 195–199.

179 M. Li, X. Zhang, Y. Zheng, Y. Xu, H. Zhang, Y. Liu and B. Lei, *Ceram. Int.*, 2020, **46**, 21560–21568.

180 H. Chen, Z. Gao, P. Lv, L. Sun and C. Xu, *J. Non-Cryst. Solids*, 2022, **597**, 121867.

181 H. Chen, T. Lin, F. Huang, S. Li, X. Tang and R. J. Xie, *Adv. Opt. Mater.*, 2022, **10**, 2200836.

182 M. Zhou, J. Sun, B. Zhang, Y. Hua, F. Huang, H. Ma, R. Ye and S. Xu, *J. Eur. Ceram. Soc.*, 2023, **43**, 3563–3571.

183 Z. Wang, Z. Yang, N. Wang, Q. Zhou, J. Zhou, L. Ma, X. Wang, Y. Xu, M. G. Brik and M. D. Dramićanin, *Adv. Opt. Mater.*, 2020, **8**, 1901512.

184 Y. Zhou, C. Yu, E. Song, Y. Wang, H. Ming, Z. Xia and Q. Zhang, *Adv. Opt. Mater.*, 2020, **8**, 2000976.

185 J. Zhou, Y. Wang, Y. Chen, Y. Zhou, B. Milićević, L. Zhou, J. Yan, J. Shi, R. S. Liu and M. Wu, *Angew. Chem.*, 2021, **133**, 3986–3991.